# Thermodynamic stability limit of the crystalline state from the Gibbs perspective

Kun Yin,* Xiancai Lu,† Huiqun Zhou, and Yicheng Sun
*State Key Laboratory for Mineral Deposits Research, School of Earth Sciences and Engineering, Nanjing University, Nanjing, Jiangsu 210023, China*

(Received 1 June 2018; revised manuscript received 17 August 2018; published 31 October 2018)

Understanding the superheating of crystals may serve as essential information for unraveling the mechanisms of homogeneous melting. Superheated crystals have been observed in experiments for decades and have broad implications in nanoscale embedded devices; however, the full extent of the metastable superheated crystalline state within equilibrium thermodynamic changes remains uncertain. Here, we investigate this problem from a geometrical perspective of the Gibbs's volume-entropy-internal energy thermodynamic surface. We find that in a homogeneous melting process, the limit of the superheated crystal can be defined as the state at which the crystal's internal energy or enthalpy, depending on whether the constraint condition is constant volume or pressure, equals the value of this property at the state where heterogeneous freezing begins. We demonstrate that the thermodynamic foundations of several different melting simulation methods, which previously were understood as mostly independent from each other, can be unified and elucidated from the same rigorous and quantitative perspective of the Gibbs surface. By tracking the trajectories of atoms relative to their equilibrium positions, we have identified the mechanisms of cooperative diffusion in the superheated face-centered-cubic Lennard-Jones crystal. Such diffusive motion is undergone in a manner that hops toward the first-nearest neighbor while keeping the crystalline structure unchanged.

DOI: 10.1103/PhysRevB.98.144113

## I. INTRODUCTION

The melting of crystals is one of the most common phase transitions and is a continuously active research area; nevertheless, the fundamental mechanisms and theories about melting are still not completely known [1–3]. A longstanding challenge regarding the melting of crystals is understanding the nature of the superheating of crystals [4–6]. Compared with other metastable phenomena of first-order phase transitions, such as the supercooling and superheating of liquids [7], the superheating of crystals is rarely observed at the macroscopic scale and is much less studied. However, it has recently been discovered that the hysteresis effect of crystals is very clear in nanoscale processes and plays a crucial role in the functioning of some materials, e.g., antifreeze proteins [8] and phase-change logic device [9]. Therefore, a more thorough understanding of the stability limits for the crystalline state is important for obtaining better insights into the mechanism of melting and for developing novel devices that can exploit the overheating properties of materials.

It is well known that at ambient pressure, the normal melting of a pure crystal, also called heterogeneous melting, typically occurs at a characteristic temperature, i.e., the melting point ($T_m$). Heterogeneous melting is preferentially initiated at free surfaces or at other defects, which are almost inevitable for most naturally occurring crystals [10–13]. Under certain circumstances, melting of the surface can be impeded by experiments [14–18]. In contrast, bulk melting starting from the interior of crystals is named homogeneous melting. One method to achieve homogeneous melting is to heat the crystal from the interior with a focused beam of light (e.g., pulsed laser), which may initiate a relatively immense superheating that lasts for only a small amount of time (∼nanoseconds) [14–16]. A transient superheating with an exceptionally high temperature can be achieved during pulsed melting due to the ultrafast heating rate; in this case, nonequilibrium intermediate states cannot be entirely excluded [2]. Another technique is to coat a single crystal with a high-melting-point layer, and with this technique, metastable superheated crystalline states have been detected under uniform thermal conditions at a much longer timescale (∼minutes) [2,17,18]. Here, we restrict our discussion to the thermodynamic changes within consistent equilibrium crystalline states. Subsequently, a fundamental question arises: During homogeneous melting, is there a threshold value for the degree of superheating beyond which the metastable solid phase is forced to melt?

The early melting theories were used to delimit the crystalline state, and the liquid state focused on phenomenological criteria [19,20]. The Lindemann criterion [19,21] states that the vibration of atoms reaches a critical fraction with respect to the neighboring distance at the instability limit. The Born criterion [20] suggests that the shear modulus of the crystal will vanish when melting occurs. However, no limit of superheating can be formulated directly from these theories. The first pioneering work that explicitly defined the stability limit of a superheated crystal was conducted by Fecht and Johnson [22]. They followed the Kauzmann argument [23] for a supercooled liquid and proposed two candidates for the superheat limit of the crystal, i.e., the isentropic and isenthalpic temperatures, at which the entropies and enthalpies of the superheated

*Corresponding author: kunyin@nju.edu.cn
†Corresponding author: xcljun@nju.edu.cn

 

crystal and the liquid phase are equal. Shortly after Fecht and Johnson, Tallon [24] introduced two additional limits by investigating the volume of a superheated crystal, and he postulated a hierarchy of catastrophes for the crystalline state and argued that the rigidity catastrophe, at which the zero rigidity coincides with the volume of the freezing point, is the ultimate bound of superheating because it preempts all other instabilities. Recently, Gallington and Bongiorno [25] hypothesized that the limits of a superheated crystal and supercooled liquid are degenerate in the enthalpy-entropy diagram, which means that the two metastable states have equal enthalpy and entropy. In addition to the above limits defined under the condition of constant pressure, Belonoshko *et al.* [26] also discovered an isochoric limit from computational simulations. They found that the internal energy of the crystal at the limit of superheating is equal to the internal energy of its liquid at $T_m$ at the same volume. This discovery has stimulated a widely used method, called the Z method, to determine $T_m$, but its physical basis is still unknown [27]. To date, many theoretical limits have been proposed [22,24–26]; nevertheless, a few key questions remain unanswered, such as what is the relationship between the limit of superheating in homogeneous melting and the equilibrium melting point in heterogeneous melting, what are the ultimate expressions for the isobaric and isochoric limits, and, more importantly, what are the perspicuous thermodynamic pictures behind these expressions?

In this work, we hypothesize that the above questions can be answered from a geometrical perspective of the thermodynamic surface initially introduced by Gibbs in 1873 [28]. To confirm this conjecture, we develop a method to construct the volume-entropy-internal energy surface for a Lennard-Jones (LJ) system [29] from computational simulations. We choose an LJ system as the model system because its thermodynamic properties can be accurately determined and easily reproduced. By investigating the phase transition paths in different thermodynamic variable spaces, we obtain expressions for the limits of superheating under isochoric and isobaric conditions simultaneously. We interpret various $T_m$-determination methods from the geometrical perspective, and we verify the proposed expressions through specifically designed molecular dynamics (MD) simulations. The superheat limit of an LJ crystal at constant pressure is calculated and compared with different previously proposed expressions. Finally, the microscopic mechanism of homogeneous melting is discussed.

## II. METHODS

### A. Construction of the Gibbs surface

In Gibbs 1873 paper [28], he introduced a three-dimensional surface, which he called the thermodynamic surface, expressing the relationship between the volume, entropy, and internal energy of a substance with an invariable composition. According to Gibbs, the equilibrium thermodynamic states of a substance with an invariable composition are regulated by the fundamental equation $dU = -PdV + TdS$, which suggests a geometrical surface in three-dimensional space, i.e., the $VSU$ surface. Once the $VSU$ surface is known, the basic properties of an equilibrium state can easily be derived, including $V$, $S$, $P$, $T$, $U$, $A$, $H$, and $G$, denoting the volume, entropy, pressure, absolute temperature, internal energy, Helmholtz free energy, enthalpy, and Gibbs free energy, respectively. Our first task is to construct the Gibbs surface with computational methods. To this end, there are two main difficulties. The first is finding an analytic form for the $U(V, S)$ function. The second relies on obtaining the values of entropy for a large number of state points. To overcome the two difficulties, we adopt a method (i.e., the Gibbs thermodynamic surface method, hereafter called the GTS method for short) to simplify this task. Rather than finding a bivariate function for the fundamental equation, we reduce our objective to finding a univariate function for $U(S)$ at a constant $V$. By differentiating the internal energy with respect to temperature at constant volume, we know that $(\partial U/\partial T)_V = C_V$, where $C_V$ is the heat capacity at constant volume. As the temperature goes to infinity, all vibrational modes in a solid are fully activated, in which case the theorem of equipartition of energy states can be applied; therefore, the heat capacity is $3k_B$ for one atom (i.e., the Dulong-Petit law), where $k_B$ is the Boltzmann constant. For temperatures that approach melting, the thermal energy is high enough versus the energy required to excite the vibrational modes, so the value of heat capacity $C_V$ is nearly constant. By differentiating the pressure with respect to temperature at constant volume, we have $(\partial P/\partial T)_V = (\partial P/\partial U)_V(\partial U/\partial T)_V = \gamma C_V/V$, in which we need to introduce the definition of Grüneisen parameter $\gamma = V(\partial P/\partial U)_V$. Based on observations in geophysical disciplines and ceramics science [30], an empirical law, $\rho\gamma =$ constant, is often used for solids with high density (e.g., oxides, silicates) at high temperatures ($T > \Theta$), where $\Theta$ is the Debye temperature evaluated by measuring acoustic velocities and $\rho$ is the density. If this law holds true, then $(\partial P/\partial T)_V =$ constant when the unit mass per particle $m$ is taken to unity (i.e., $m = 1$, $V = 1/\rho$). A general theory of the heat capacity and Grüneisen parameter of liquids has not been established. Here, we just assume that their behavior near the phase-transition temperature is similar to that of the solid, which is consistent with our findings of the $P$-$V$-$T$ and $U$-$V$-$T$ relationships in the molecular dynamics simulations. As a result of the above justification of assumptions, when temperature is not far from $T_m$, $(\partial U/\partial T)_V$ and $(\partial P/\partial T)_V$ can be approximately regarded as constants. Therefore, we assume that the internal energy and pressure change linearly with temperature under isochoric conditions. These assumptions are mostly adequate when studying the solid-liquid transition of LJ systems within the pressure range investigated in this work. First, at temperatures around the melting point, we can assume that the internal energy is linearly dependent on the temperature under a constant volume condition, which is

$$U(T)|_{V=\text{constant}} = aT + b. \tag{1}$$

By substituting $T = (\partial U/\partial S)_V$ into Eq. (1), we derive the $U(S)$ function at constant volume:

$$U(S)|_{V=\text{constant}} = c \times \exp(S/a) + b. \tag{2}$$

In principle, with the knowledge of the coefficients $a$, $b$, and $c$ in Eq. (2) for a number of different constant volumes, the Gibbs surface can be constructed. Among the three

coefficients, $a$ and $b$ can be determined by fitting Eq. (1) to the results of canonical ensemble (i.e., NVT ensemble) MD simulations. By choosing a reference state on the surface, $c$ can be calculated using the following equation:

$$c = \frac{aT_r}{\exp\left[(aT_r+b) - U_r + T_r S_r + \int_{V_r}^{V} p(V)dV\right] - \exp(aT_r)}, \tag{3}$$

where $V$ is one volume in the set of constant volumes; $V_r$, $T_r$, $U_r$ and $S_r$ are the volume, temperature, internal energy, and entropy at the reference state, respectively; $a$ and $b$ are the same as in Eq. (1); and $p(V)$ is a function at the constant reference temperature $T_r$, which is determined by fitting a number of volume-pressure data pairs to an empirical isothermal equation of state (EOS). The volume-pressure data pairs can be obtained from fitting the linear $P(T)$ relations at different volumes. To construct the Gibbs surface for a single phase, the absolute position of the reference state is immaterial; however, for determining the phase transition of two phases, a constant shift should be made along the entropy axis to ensure that the primitive surfaces of the two phases share the same zero point. The amount of entropy shift ($\delta S$) can be determined in a variety of ways that require some additional methods [31–34]. In these ways, only one or two states containing the information of entropy must be known beforehand, which greatly reduces the effort in the calculations of entropy or free energy. More details on the choice of the reference state and the entropy calibration are presented in the Supplemental Material (SM) [35].

### B. Details of molecular dynamics simulations

The classical MD simulations in this work are performed using the LAMMPS package [36]. The interparticle interaction of the system is governed by the LJ potential [29]:

$$\phi(r) = 4\varepsilon\left[\left(\frac{\sigma}{r}\right)^{12} - \left(\frac{\sigma}{r}\right)^{6}\right], \tag{4}$$

where $r$ is the interparticle distance and $\sigma$ and $\varepsilon$ are parameters of the potential. In this work, all quantities are reported in reduced units; for example, the units of volume, entropy, energy, pressure, temperature, density, and time are $\sigma^3$, $k_B$, $\varepsilon$, $\varepsilon/\sigma^3$, $\varepsilon/k_B$, $\sigma^{1/3}$, and $(m\sigma^2/\varepsilon)^{1/2}$, respectively. In reduced units, $\sigma = \varepsilon = m = k_B = 1$. In real units, $\sigma$, $\varepsilon$, $m$, and $k_B$ are replaced by the corresponding physical values of a particular material (e.g., $\sigma = 3.405 \times 10^{-10}$ m, $\varepsilon = 1.654 \times 10^{-21}$ J, $m = 6.634 \times 10^{-26}$ kg for argon).

#### 1. GTS method calculations

The GTS method calculations are performed using a series of NVT ensemble MD simulations with the Nosé-Hoover thermostat. Seven different densities are sampled for each phase ($\rho$ = 0.90, 0.95, 1.00, 1.05, 1.10, 1.15, and 1.20 for the solid phase, and $\rho$ = 0.80, 0.85, 0.90, 0.95, 1.00, 1.05, and 1.10 for the liquid phase). At each density, five temperatures are sampled. Accordingly, 70 different thermodynamic states have been sampled altogether. For each single state, the system is run 30 000 time steps under periodic boundary conditions with a time step of $1.25 \times 10^{-3}$. (If the parameters of argon are replaced in the reduced units, the corresponding time step is 2.725 fs.) The first 20 000 steps are used for equilibration. The remaining steps are averaged to obtain the equilibrium properties. The initial configuration of the system is a $5 \times 5 \times 5$ supercell of the face-centered-cubic (fcc) lattice, which contains 500 particles. The liquid configuration is achieved by heating the solid system to a high temperature that ensures complete melting. The long-range interactions are included using the Ewald method. We use the fourth-order virial expansion equation to represent the $p(V)$ relation in Eq. (3). The entropy is calibrated using a fixed point on the melting curve. The following values are used for the reference state: $\rho_r = 0.90$ ($V_r = 1.11$), $S_r = 8.200$, and $T_r = 2.081$ for the solid phase, and $\rho_r = 0.80$ ($V_r = 1.25$), $S_r = 7.781$, and $T_r = 1.067$ for the liquid phase.

#### 2. Z method calculations

The Z method was proposed by Belonoshko *et al.* [26] in 2006 and received its name from the characteristic shape of the isochore plotted on the pressure-temperature diagram. In this method, the system starts from a perfect lattice configuration, and the simulation is performed in the microcanonical ensemble (i.e., NVE ensemble). While keeping the volume constant, the kinetic energy of the system is gradually increased. By projecting the pressure-temperature data pairs of the system onto a two-dimensional diagram as the kinetic energy is increased, we can trace the pathway that the system underwent. The pathway first increases in a solid-state region. It crosses the melting curve and then enters the superheating region while preserving a metastable solid state. The magnitude of the kinetic energy eventually exceeds a critical value at which the system suddenly melts, and the values of pressure and temperature of the system exactly drop down to the melting curve. The state of the system when it reaches the critical total energy is called the limit of superheating. The temperature at the superheating limit is defined as $T_{LS}$. On further increase in the kinetic energy, the pathway increases again in the liquid-state region. Finally, the points belonging to this pathway form an isochore with a shape that looks similar to the letter Z. By observing the behavior of the energy increasing process, the authors discovered an important relation: at the same volume, the total energies at the limit of the superheating of the solid branch and at the equilibrium melting point of the liquid branch are equal. This can be written as the following equation:

$$U^{\text{solid}}(V, T_{LS}) = U^{\text{liquid}}(V, T_m). \tag{5}$$

The Z method calculations in this study are performed at a constant volume of $V = 0.9614$ (the corresponding density is $\rho = 1.0402$). The initial configuration of the system is built from a $5 \times 5 \times 5$ supercell of a perfect fcc crystal that contains 500 particles. The total number of time steps is 0.4 million with a time step $1.14 \times 10^{-4}$ (equivalent to 0.25 fs if the system is substituted by argon). A number of MD simulations with different constant internal energies are run under the NVE ensemble. In each run, the system is provided with an initial kinetic energy, which is determined by the initial temperature. Therefore, the total energy of the system is tuned by specifying the initial temperature, which is set

to be approximately twice the desired temperature, in the form of the normal distribution of particle velocities. Then, the system evolves under a constant internal energy without any external intervention until it reaches full equilibrium. The last $\frac{1}{10}$ length of the simulation is averaged to obtain the equilibrium properties. To identify the drop in temperature from the superheat limit ($T_{LS}$) to the equilibrium melting point ($T_m$) described in Eq. (5), we perform two rounds of MD simulations. The first round of simulations is performed around an initial guess of the melting point and sampled by a few state points using a coarse temperature interval ($\Delta T = 0.1$). A discontinuity in internal energy (or pressure) can be identified after the first round of simulations. The second round of simulations is performed around the discontinuity identified in the first round, and the state points are sampled using a fine-temperature interval ($\Delta T = 0.01$).

#### *3. Isobaric-isenthalpic ensemble calculations*

The isobaric-isenthalpic ensemble (constant pressure and constant enthalpy ensemble), also called the NPH ensemble, calculations are performed under a constant pressure of $P = 5.0$. The procedure of this method is similar to that of the Z method, except that the enthalpy of the system is kept as a constant rather than the internal energy. We start from a perfect fcc crystal with 500 particles in the simulation box. A number of MD simulations with different constant enthalpies are run under the NPH ensemble. The idea is simply to rescale the initial velocities of the particles and let the system equilibrate freely under constant $N$, $P$, and $H$. The initial velocities are determined by an initial temperature, which is twice the desired temperature (the equilibrium temperature after the simulation will be approximately the desired temperature but not necessarily the same). The NPH ensemble simulation is performed under a given hydrostatic pressure. To avoid the enthalpy (i.e., energy) drift that typically occurs in a long simulation, we provide the time step a sufficiently small value. The total number of time steps is 1.6 million with a timestep of $5.7 \times 10^{-5}$ (equivalent to 0.125 fs if the system is substituted by argon). The last 0.2 million steps are averaged to obtain the equilibrium properties. To identify the drop in temperature from the superheating limit to the equilibrium melting point, we perform three rounds of MD simulations with a minimum temperature interval $\Delta T = 0.002$.

### C. Microscopic motion analysis

When analyzing the microscopic motion of atoms in the simulation, there are two distinct approaches: one is the atom-focused observation, and the other is the position-focused observation. Here, we use camera shooting as an analogy to explain the difference between the two approaches. The atom-focused observation refers to tracking a certain atom with a moving camera. We take consecutive images at regular intervals and calculate the displacement of the atomic coordinates over time from the images. The atom's hopping information is obtained by examining whether the atomic displacement exceeds a given threshold between two configurations. The position-focused observation is to keep the camera still, so that it is focused on a certain reference position (i.e., one of the equilibrium or ideal positions of the crystalline sites). Similarly, images are taken at regular intervals. After each image is taken, we calculate the distances between all atoms in the field of view and the reference position. The atom with the smallest distance is defined as the occupant of the reference position at this moment. The hopping information of the atom is obtained by observing the flow of the occupant.

The main disadvantage of the atom-focused observation is that some parameters need to be specified artificially, and these parameters will seriously interfere with the accuracy and uniqueness of the analysis results. The first parameter is the threshold of the atomic displacement, which is the criterion for determining whether an atom has hopped. The choice of this threshold is somewhat empirical and technical. Some *a priori* knowledge of the relative amplitude of the atomic vibration with respect to the nearest-neighbor distance is needed. To set a reasonable value, many trials are needed since a minor change in this parameter can cause a large statistical deviation in the analysis results. Moreover, the threshold also needs to be adjusted according to volume changes (such as thermal expansion), which will also require artificial interference. The second parameter is the time interval for calculating the atomic displacement between two configurations. The choice of this time interval has a great impact on the result because the duration of atomic hopping is on a timescale equivalent to this interval. If this time interval is set too small, a hopping may be missed since the displacement will be too small to be recorded.

However, the position-focused observation does not require an artificial parameter of the displacement threshold; and the time of the atomic hopping is small enough compared to the time at which the atom occupies a certain position, which makes the information that is acquired in this way insensitive to the setting of the observation time interval. Therefore, the second way yields results that are more reliable and less ambiguous, and the results of this approach are more convenient for subsequent quantitative analysis and visualization. In this paper, we use the position-focused way to analyze the microscopic motion of atoms in superheated crystals.

## III. RESULTS AND DISCUSSION

### A. Transition paths and metastability limits

In the $TPG$ space, the coexistence of two phases is represented by the crossing curve of the primitive $TPG$ sheets of the two phases. Projecting the crossing curve onto the temperature-pressure plane results in the so-called melting curve [solid curve in Fig. 1(a)]. The intersection point of two $TG$ curves in an isobaric plane [point E in Fig. 1(b)] is the melting point ($T_m$) defined for heterogeneous melting at constant pressure. This geometrical picture is exactly what the following expression reflects:

$$G_{\mathrm{E}}^{\mathrm{solid}}(P, T_m) = G_{\mathrm{E}}^{\mathrm{liquid}}(P, T_m). \tag{6}$$

From Gibbs perspective, a single point on the melting curve [square in Fig. 1(a)] diverges into a common tangent line in spaces other than $TPG$, which is shown as a solid straight line in Figs. 1(c) and 1(e). In this way, the original superposed but inherently different coexisting states represented by a crossing curve in the $TPG$ space will be distinctly represented by a developable surface in the $VSU$ space or

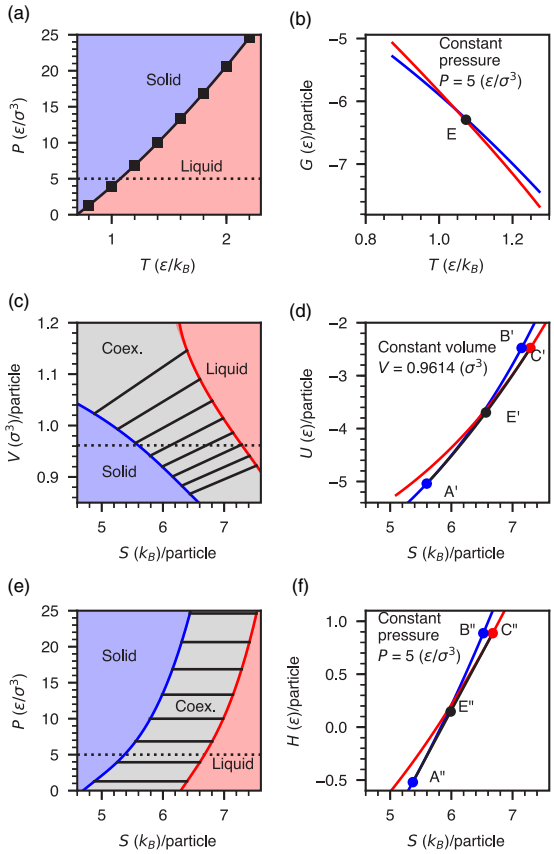


FIG. 1. Solid-liquid phase transition boundaries and paths of the LJ system presented from different perspectives. View from the (a) temperature-pressure diagram, (b) temperature-Gibbs free energy diagram, (c) entropy-volume diagram, (d) entropy–internal energy diagram, (e) entropy-pressure diagram, and (f) entropy-enthalpy diagram. Point E represents a heterogeneous melting point. Paths A′C′ and A″C″ are the stable regimes of the coexisting states of two phases. Points E′ and E″ designate arbitrary points moving reversibly along A′C′ and A″C″ during a heterogeneous process. Paths A′B′ and A″B″ are the superheated metastable solid regimes. Points A′ and A″ are the lower termini of coexisting states that are in a complete crystalline phase. Points C′ and C″ are the upper termini of coexisting states that are in a complete liquid phase. Points B′ and B″ are the limits of superheated crystalline states during a homogeneous process. Color scheme: crystalline solid phase (blue), liquid phase (red), and coexistence of two phases (black).

$SPH$ space. Their projections onto the horizontal planes are shown as gray shaded areas in Figs. 1(c) and 1(e). The boundaries of the shaded areas are called the limit of absolute stability by Gibbs, and they are formed by the terminal points of the common tangent lines.

By investigating the geometrical paths in the isochoric plane of $VSU$ space [Fig. 1(d)] and the isobaric plane of $SPH$ space [Fig. 1(f)], thermodynamic expressions comparable to Eq. (6) can be established to locate the limit of metastability. In Figs. 1(d) and 1(f), two phase transition situations are shown: (i) If the initial configuration of the system is heterogeneous, which means that the system has some type of imperfectness that disrupts the neat arrangement of crystal sites (e.g., free surfaces, interfaces, dislocations, grain boundaries, and so forth), the phase transition will pass through the most stable states that always possess the maximum value of entropy. The intermediate states during the transition along the path A′-E′-C′ or the path A″-E″-C″, representing the coexistence of two phases, can change slowly and reversibly. (ii) If the initial configuration is homogeneous, which means that the crystal has a uniform nature throughout in composition and structure without a free surface, the phase transition will be hindered due to the energy barrier to form a critical-size nucleus. The system can persist in the metastable regime until its internal energy or enthalpy reaches a critical value that equals the value at the terminus of the coexisting state. After reaching the critical value, a spontaneous transition from the metastable state to the stable state is forced to occur. In contrast to the heterogeneous process, this transition occurs catastrophically and irreversibly. The state immediately before this transition is defined as the limit of metastability.

Consequently, depending on the constant condition constraint, two thermodynamic expressions can be derived:

$$U_{\mathrm{B}'}^{\mathrm{solid}}\left(V, T_{l+}^{\mathrm{u}}\right) = U_{\mathrm{C}'}^{\mathrm{liquid}}(V, T_{m+}), \tag{7}$$

$$H_{\mathrm{B}''}^{\mathrm{solid}}\left(P, T_{l+}^{\mathrm{h}}\right) = H_{\mathrm{C}''}^{\mathrm{liquid}}(P, T_{m}). \tag{8}$$

In Eqs. (7) and (8), the first quantity in the parentheses is the constraint condition. $T_{l+}^{u}$ and $T_{l+}^{h}$ denote the temperatures at the limit of the superheated crystal under isochoric and isobaric conditions, respectively. In the isochoric condition, the transition is from point B′ to point C′. As the isochoric plane passes through different common tangent lines in Fig. 1(c), A′C′ is a curved line with varying tangents, as shown in Fig. 1(d). Therefore, the temperature at point C′ is higher than the temperature of other points on A′C′. To distinguish this temperature from other melting points, it is denoted as $T_{m+}$ in Eq. (7). In the isobaric condition, the transition is from point B″ to point C″. The isobaric plane passes through only one common tangent line in Fig. 1(e), and A″C″ is a straight line with a single slope. Therefore, the temperatures of all melting points on A″C″ are identical and denoted as $T_m$ in Eq. (8).

The thermodynamic variables used to plot Fig. 1 for the solid and liquid LJ system were calculated with the coefficients of Eq. (2) derived from the computational approach introduced in Sec. II A and the SM [35] of this study, i.e., the GTS method. Values of the thermodynamic variables at points A′, A″, B′, B″, C′, C″, and E are listed in Table I. Point E actually represents a number of superimposed thermodynamic states that, although having the same pressure and temperature, are completely different. In Table I, we list the values of the thermodynamic variables of point E in the two end states, namely, the completely solid state and completely liquid state. The former state is equivalent to the thermodynamic state represented by point A″, while the latter is equivalent to the state represented by point C″. In principle, they should have equal thermodynamic variables, but, in fact, their data have a slight difference in Table I. This is because the initial natural variables are different in the four thermodynamic potentials (i.e., $U$, $A$, $H$, $G$), so numerical errors are caused by the different sequence of thermodynamic potentials used when calculating thermodynamic variables of different states. To our knowledge, $VSU$ surfaces were only constructed using

TABLE I. Values of the thermodynamic variables at points A′, A″, B′, B″, C′, C″, and E.

| | $V$ ($\sigma^3$) | $S$ ($k_B$) | $P$ ($\varepsilon/\sigma^3$) | $T$ ($\varepsilon/k_B$) | $U$ ($\varepsilon$) | $A$ ($\varepsilon$) | $H$ ($\varepsilon$) | $G$ ($\varepsilon$) |
|---|---|---|---|---|---|---|---|---|
| A′ | 0.9614 | 5.597 | 7.372 | 1.235 | −5.042 | −11.952 | 2.046 | −4.864 |
| B′ | 0.9614 | 7.148 | 14.597 | 2.156 | −2.478 | −17.887 | 11.555 | −3.854 |
| C′ | 0.9614 | 7.292 | 17.070 | 1.809 | −2.477 | −15.668 | 13.934 | 0.744 |
| A″ | 0.9821 | 5.370 | 5.000 | 1.073 | −5.431 | −11.192 | −0.520 | −6.281 |
| B″ | 1.0450 | 6.522 | 5.000 | 1.365 | −4.338 | −13.243 | 0.887 | −8.019 |
| C″ | 1.0721 | 6.675 | 5.000 | 1.075 | −4.474 | −11.647 | 0.887 | −6.287 |
| E[a] | 0.9821 | 5.370 | 5.004 | 1.073 | −5.430 | −11.192 | −0.516 | −6.278 |
| E[b] | 1.0727 | 6.675 | 4.969 | 1.073 | −4.477 | −11.639 | 0.854 | −6.309 |

[a]The end state of point E in a completely solid phase.
[b]The end state of point E in a completely liquid phase.

experimental data previously, either by hand [37] or by computer visualization [38]; this work is the first in which a $VSU$ surface is constructed completely from theoretical calculation.

### B. Interpretations of methods in melting simulations

In the realm of computational methods of melting simulation, it was long ago recognized that the heat-until-melts (HUM) method would significantly overestimate the melting point ($T_m$) because of the hysteresis effect during the first-order phase transition [39]. A straightforward approach to determine the $T_m$ that intrinsically overcomes the hysteresis problem is based on the thermodynamic definition of $T_m$ [Eq. (6)]. This category of methods requires calculating the free energies of the solid phase and liquid phase as functions of temperature at a given pressure; therefore, it is often termed the free-energy method. Although it has a strict thermodynamic basis, the full implementation of the free-energy method from first principles has been restricted to a small number of simple systems (e.g., monoatomic materials) due to the complex setup and high-precision demand of such methods [40,41]. The second category of methods is based on inspecting the dynamical evolution of the system under certain constrained external conditions. Different statistical ensembles have been used to predict $T_m$ in practical simulations [26,42–44]. According to the initial configuration of the system setup, that is, whether the solid-liquid interface exists in the initial system, such methods can be classified as two-phase (or coexistence) methods and one-phase methods. In addition, there is also a third category of methods that acts as a bridge between the first two categories of methods. Such a third method is called the reference coexistence method [45,46] and essentially consists of performing two-phase coexistence simulations with a reference energy model and, subsequently, performing thermodynamic integration via free-energy concepts all the way up to the energy model of interest. So far, the different simulation melting methods were understood mostly independently from one another. In the following part, we unify and elucidate the underlying thermodynamic foundations for some of these methods in the second category from the same rigorous and quantitative perspective.

First, if the initial configuration of the method has only one phase, then it is called a one-phase method. The method developed by Belonoshko *et al.* [26] is an example of such a method. Following the computational procedure of this method, a "Z"-shaped isochore will appear in the pressure-temperature diagram (hence, it was named the Z method), and the lower turn point of the isochore exactly drops to the melting curve and has internal energy equivalent to that of the higher turn point of the isochore (Fig. 2). Based on this surprising behavior discovered in the NVE ensemble simulations, an empirical formula that defines the isochoric limit of superheating was established [see Eq. (5)]. Belonoshko *et al.*'s formula is essentially identical to the equation that we proposed in Eq. (7), but the latter reveals more information. From Eq. (7), we know that (i) the melting point found by the Z method is actually point C′ in Fig. 1(d), at which the liquid phase has the maximum melting temperature ($T_{m+}$) on the curve A′C′ and starts to freeze heterogeneously when the temperature is lowered further; (ii) the superheat limit $T_{LS}$ defined in the Z method is actually the temperature of point B′ in Fig. 1(d), which has the same internal energy as point C′; and (iii) the "Z"-shaped isochore is just the manifestation of the path A′-B′-C′, which represents the homogeneous melting under constant volume conditions, on the pressure-temperature diagram.

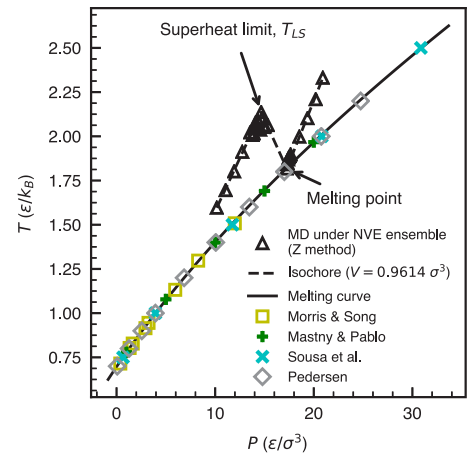


FIG. 2. Illustration of the Z method calculations for the LJ system. The results of MD simulations under the NVE ensemble (constant volume, $V = 0.9614\ \sigma^3$) are shown as triangles. The melting curve is obtained from the GTS method of this study, which is in good agreement with previous calculations by Morris and Song [47], Mastny and Pablo [48], Sousa *et al.* [49], and Pedersen [50].

After we know that the thermodynamic relation expressed in Eq. (7) can be observed in the NVE ensemble simulations, which has been confirmed by calculations with the Z method, we may envision a similar one-phase method to be performed in the NPH ensemble, through which the relation expressed in Eq. (8) will be observed. According to the path A″-B″-C″ in Fig. 1(f), which represents homogeneous melting under constant pressure conditions, it is expected that the crystal should melt at the isobaric limit of superheating; then, in the pressure-temperature diagram, it should suddenly drop to a point on the melting curve, whereas in the volume-temperature diagram, it should drop to a point on the liquid branch of the limit of absolute stability. The two states between the drops should have equivalent enthalpy. Note that in the theory of Tallon's rigidity criterion [24], this equivalent quantity is hypothesized to be volume. To check this hypothesis with the LJ system, we first predict the melting point $T_m$, the limit of superheating $T_{l+}^h$ defined in Eq. (8), and the limit of superheating $T_m^r$ defined by Tallon, which are shown as circles, squares, and diamonds, respectively, in Figs. 3(a) and 3(b). Then, we perform a series of one-phase MD simulations at a constant pressure ($P = 5.0\ \varepsilon/\sigma^3$) under the NPH ensemble. We find that the equilibrium properties of the MD simulations, shown as triangles in Fig. 3, indeed drop to $T_m$ from $T_{l+}^h$ rather than from $T_m^r$.

This finding supports our proposition in Eq. (8). We have derived the limit of absolute stability for the LJ system from the Gibbs thermodynamic surface approach and plotted it in the entropy-volume diagram [Fig. 1(c)] and entropy-pressure diagram [Fig. 1(e)]. Now, drawing the limit of absolute stability on the volume-temperature diagram [Fig. 3(c)] shows a very good agreement with previous calculations [48–50]. Similar to the isochore formed in the pressure-temperature diagram of the Z method calculations, the isobar of the NPH ensemble calculations in Fig. 3(c) also exhibits a "Z" shape in the volume-temperature diagram. As we expected, the lower turn point of the isobar lies exactly on the liquid branch of the limit of absolute stability. Thus, this simulation method can be used as a new Z method analogous to the original Z method but performed in the NPH ensemble. We have tested the effects of system size and duration of simulations on the new method. The results show that the Z method under constant pressure has a simple running process and can be applied to a small system (e.g., 256 atoms); therefore, it is ideally suitable to be performed by *ab initio* molecular dynamics simulation. The main problem of this method is that, as pointed out by Alfè *et al.* [27], the waiting time (a time before melting occurs) strongly depends on the excess energy of the crystal above the superheating limit and on the system size. This problem makes it difficult to estimate a sufficient time to wait for a melting to occur in the simulation. If the simulation time is too short to exceed the waiting time, the final liquid temperature will be overestimated. However, the probability distribution of waiting time is consistent with a rare-event process. The sufficiency of the simulation length and the location of superheating limit are difficult to evaluate from the method itself. In some cases (e.g., high pressure), the waiting time may be exceptionally long [51].

Second, if the initial configuration of the method has a predefined solid-liquid interface, it is termed a two-phase (or

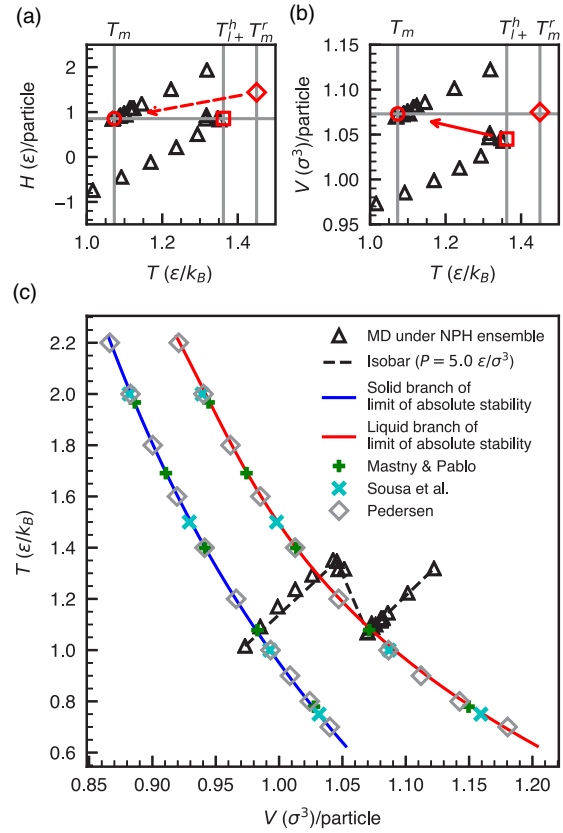


FIG. 3. Illustration of the one-phase MD simulations of the LJ system under the NPH ensemble. (a) View from the temperature-enthalpy diagram, (b) view from the temperature-volume diagram, and (c) a broader view from the temperature-volume diagram showing the limit of absolute stability altogether. $T_m$, $T_{l+}^h$, and $T_m^r$ are the temperatures at the melting point, the isobaric limit defined in this work, and the rigidity limit defined by Tallon [24], respectively, which are correspondingly marked as circles, squares, and diamonds in (a) and (b). The MD simulations are performed at the constant pressure $P = 5\ \varepsilon/\sigma^3$, and the results are shown as triangles. The solid branch (blue line) and liquid branch (red line) of the limit of absolute stability are obtained from the GTS method of this study, and they are in good agreement with previous calculations by Mastny and Pablo [48], Sousa *et al.* [49], and Pedersen [50].

coexistence) method [42–44,52]. In reality, there are various implementations of this method. If the value of the internal energy is properly chosen in the case of the NVE-ensemble implementation, then after evolving to an equilibrium melting point, there are still two phases that coexist in the system. By altering the internal energy (or volume), a new equilibrium point on the melting curve will be established. When the internal energy exceeds the proper interval, the coexisting system will completely transform into a single phase [42]. Another widely used two-phase approach is implemented in the isobaric-isothermal ensemble (i.e., NPT ensemble), where irrespective of how close the temperature approaches the melting point, only a single phase (either solid or liquid) can be observed in the final equilibrium system. Thus, the melting point can be bracketed only by progressively narrowing the upper and lower temperature bounds [43]. In addition to the above two commonly used approaches, implementations of

the two-phase method in the NPH ensemble [44] and NVT ensemble [53] are also occasionally used.

In practice, numerous studies have successfully determined the $T_m$ using variations of the two-phase method; however, the underlying thermodynamic origins of these methods have not yet been clearly interpreted in a unified framework. Here, we want to emphasize that they are merely different manifestations of the two heterogeneous melting paths [i.e., the paths A′-E′-C′ in Fig. 1(d) and A″-E″-C″ in Fig. 1(f)] in different statistical ensembles. Therefore, it is easy to understand why a coexisting phase in the final equilibrium state of the NVE [42], NPH [44], or NVT [53] ensemble simulations is expected to be observed, while only a single phase is observed in the case of the NPT ensemble simulation [43]. The reason for this result lies in the fact that in the former three cases, the system is stable within a finite thermal interval (i.e., internal energy interval or enthalpy interval), but in the NPT case, the system can be stable only at a single temperature; therefore, an infinitesimal thermal fluctuation is sufficient to alter its state. Moreover, it is understandable why coexistence may occur over a small range of temperatures in the NVE or NVT ensemble simulations but occurs only at a single temperature in the NPH ensemble simulations. The reason for this behavior has been incorrectly attributed to the finite-size effect [42]; however, as we explained in the previous section, this behavior is actually based on the tangents of the transition paths A′C′ and A″C″. In this view, the melting points determined by different approaches, although they all fall on the melting curve, may represent completely different states. To confirm this view, we slice an isochoric plane in the $VSU$ space. We first predict the right interval where the two phases can coexist. Then, we perform a series of two-phase MD simulations under the NVE ensemble using different internal energies between the predicted interval. The phase separation is distinguished by the coloring of liquidlike and solidlike particles whose colors are associated with their local bond orientational order parameters [54]. After the evolution, as expected, the proportion of the two phases and the equilibrium properties are all in good agreement with our predictions (SM [35]).

### C. Comparison with other theoretical limits

As we mentioned in Sec. I, until now, only a few thermodynamic expressions could be written to define the temperature at the limit of superheating [22,24–26]. Comparing the different theoretical limits for the LJ system would be interesting. In the case of the constant volume condition, we have shown that our isochoric criterion defined in Eq. (7) is equivalent to Belonoshko *et al.*'s criterion [26]. In the case of the constant pressure condition, we have calculated the various isobaric limits for the LJ system at a fixed pressure ($P = 5.0\,\varepsilon/\sigma^3$). As shown in Fig. 4(g), the isobaric limits pertaining to different criteria are structured in a hierarchical order: from the outermost to the innermost are Fecht and Johnson's isentropic temperature ($T_i^s$) [Fig. 4(a)], Tallon's isochoric temperature ($T_m^v$) [Fig. 4(c)], Fecht and Johnson's isenthalpic temperature ($T_i^h$) [Fig. 4(b)], Tallon's rigidity temperature ($T_m^r$) [Fig. 4(d)], our isenthalpic temperature ($T_{l+}^h$) [Fig. 4(f)], and Gallington and Bongiorno's degenerate temperature ($T_s$) [Fig. 4(e)]. Here,

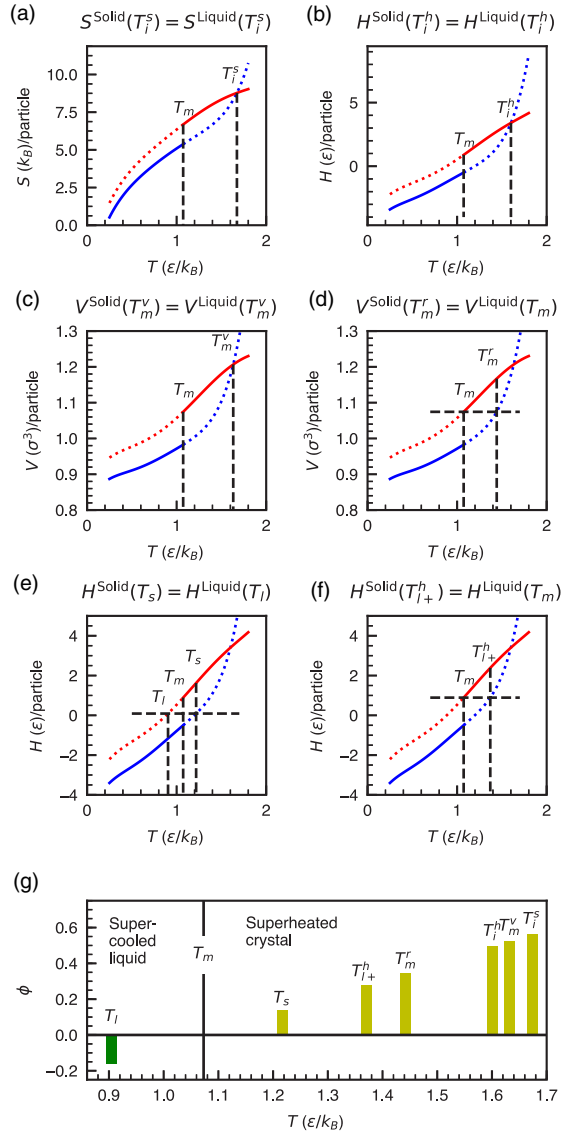


FIG. 4. The entropy, enthalpy, and volume of liquid and crystalline LJ systems as functions of temperature in the stable and metastable regimes at a constant pressure ($P = 5\ \varepsilon/\sigma^3$). Data are obtained from the GTS method of this study. The temperatures at the isobaric limit of superheating are determined according to the following criteria: (a) Fecht and Johnson's isentropic criterion, $T_i^s$ [22]; (b) Fecht and Johnson's isenthalpic criterion, $T_i^h$ [22]; (c) Tallon's isochoric criterion, $T_m^v$ [24]; (d) Tallon's rigidity criterion, $T_m^r$ [24]; (e) Gallington and Bongiorno's degenerate criterion, the limit of superheating $T_s$, and the limit of supercooling $T_l$ [25]; (f) this work's isobaric criterion defined in Eq. (8), $T_{l+}^h$; and (g) a hierarchical view of all previous temperatures, in which $\phi = (T - T_m)/T_m$ defines the ratio of the overheating or undercooling magnitude to the equilibrium melting temperature $T_m$. Color and line schemes: crystalline phase (blue line), liquid phase (red line), stable phase (solid line), and metastable phase (dotted line); the dashed horizontal and vertical lines are guides for the eye.

$T_{l+}^h$ denotes our result calculated according to Eq. (8). Our temperature is the innermost bound among all these limits except $T_s$. It is clear that $T_s$ is lower than $T_{l+}^h$ because the tangent at Gallington and Bongiorno's degenerate point [i.e., the

crossing point of the red curve and the blue curve in Fig. 1(f)] is smaller than the tangent at our superheating limit [i.e., point B″ in Fig. 1(f)]. However, Gallington and Bongiorno's criterion requires the phase transition to occur directly between a superheated crystalline state and a supercooled liquid state. It is difficult to imagine why the system can overcome the free-energy barrier of nucleation and transform into another metastable state, but it does not change to a more stable coexistence state under that condition. We conjecture that the state at $T_s$, as the limit of the crystalline state, is practically invisible in both simulations and experiments.

Lu and Li [55] proposed a kinetic limit based on the analysis of homogeneous nucleation behavior for melting in superheated crystals. They compared the various foregoing isobaric limits with their kinetic limit for aluminum and found that the instability temperature defined by the homogeneous nucleation catastrophe is the lowest one, which occurs slightly earlier than Tallon's rigidity catastrophe. The tendency of the kinetic limit for aluminum is quite similar to our isobaric limit for the LJ system. Verifying whether this is a coincidence or whether there is a close connection between the two limits is a very interesting topic. In addition, Jin *et al.* [56] monitored the atomic-scale motions of a surface-free LJ crystal during melting using MD simulations and revealed a simultaneous violation of both Lindemann's vibrational criterion [19] and Born's shear modulus criterion [20] at the kinetic limit. If the limit that we proposed in this work from the thermodynamic perspective indeed coincides with the kinetic limit based on the classical homogeneous nucleation theory, then it would imply that the thermodynamic, kinetic, vibrational, and mechanical limits actually converge in a homogeneous melting process.

### D. Microscopic mechanism of homogeneous melting

For heterogeneous melting, the crystals are melted via a nucleation process. In the nucleation process, small nuclei of the product phase form in the parent phase by thermal fluctuations. According to the classical nucleation theory (CNT), if the size of the nuclei exceeds a critical radius, they tend to grow larger; otherwise, they tend to shrink. Atoms at the surfaces or other defects have a higher free energy than those in a perfect crystal. All kinds of defects facilitate to lower the free-energy barrier in CNT; therefore, heterogeneous melting takes place preferentially at the defective sites (e.g., free surfaces, grain boundaries, dislocations, vacancies, interstitials). However, CNT is not fully applicable for homogeneous melting in defect-free crystals. According to a direct observation of the homogeneous nucleation process in melting for the colloidal system by Wang *et al.* [57], the homogeneous melting process can be divided into two stages: the incubation stage and the nucleus growth and coalescence stage. During the incubation stage, the superheated crystals still maintain a complete crystalline structure and there is no formation of a critical liquid nucleus in the crystal. Wang *et al.* [57] found that CNT can be applied for weak superheating in the second stage, but it would fail to explain the formation of multimer attachment at strong superheating in the second stage and fail to predict the types of nucleation precursors in the incubation stage.

The microscopic mechanism of the initial incubation stage of homogeneous melting is still under debate. The controversy is mainly about the form of nucleation precursors. In the atomic system, current experimental methods are unable to obtain this information because this stage occurs on very small spatial and temporal scales. As an alternative, computer simulation showed that various types of nucleation precursors are possible [58–62]. In this study, we analyzed the microscopic motions of atoms using the position-focused method introduced in Sec. II C. Three concepts are used to monitor the hopping history of all atoms on a series of observed images and are named the Position-ID, Atom-ID, and Image-ID. The Position-ID is the index of the idealized atomic coordinate in the perfect crystal. The Atom-ID is the index of each atom. The Image-ID is the index of the image in the order of observation. All indices are counted from 0. The output file stores information about the initial atom and all subsequent changes of atoms in a position and the changing moment (i.e., at which Image-ID, which Atom-ID moves out or moves in some Position-ID). The information recorded in the above format can be easily converted into the DOT language. After processing by the graph visualization software GRAPHVIZ [63], we can draw a picture containing all the atoms that have hopped and the relationship between them. The picture is named the hopping map (Fig. 5). In the hopping map, a position is represented by a box, an atom is represented by a circle, and they are connected by a line with an arrow. The direction of the arrow represents the direction of the atom's movement. An arrow from the box to the circle means an atom is leaving the position, otherwise indicating entering the position. The labels in the box and circle represent Position-ID and Atom-ID, respectively, and the labels on the edge of the line represent Image-ID, which also indicate the time sequence when the hopping occurs. The advantage of drawing such a graph is that it is easy to distinguish between atoms belonging to different hopping clusters, and furthermore the hopping order and cooperation of atoms in each cluster can be clearly identified. We can also selectively slice a fragment from the hopping cluster, highlight the atoms in the fragment on each frame of image, and finally generate a movie. In this way, the microscopic process of the cooperative movement of these atoms can be visually observed.

Based on the observation of the hopping map and movie and the analysis of the atomic coordinates involved in hopping, we can now summarize the following findings:

(1) For deeply superheated crystals, atoms are able to move collectively in a diffusive way in addition to vibrations near the equilibrium positions.

(2) At least for the system of this study (i.e., the fcc LJ crystal), the unit step of the diffusive motion of an atom is performed in a manner that hops toward the first-nearest neighbor (1NN) with a timescale on the order of 0.1 to 1.0 ps.

(3) According to the final position of the atomic hopping, it can be divided into an unstable hopping and a stable hopping. Unstable hopping may also be called temporary hopping and means that the atom returns to the original position very quickly after hopping [Fig. 5(a)]. Stable hopping, also known as permanent hopping, means that the atom stays in a new position stably after hopping [Fig. 5(b)]. We can think of a temporary hop as a failed attempt to make a permanent hop.

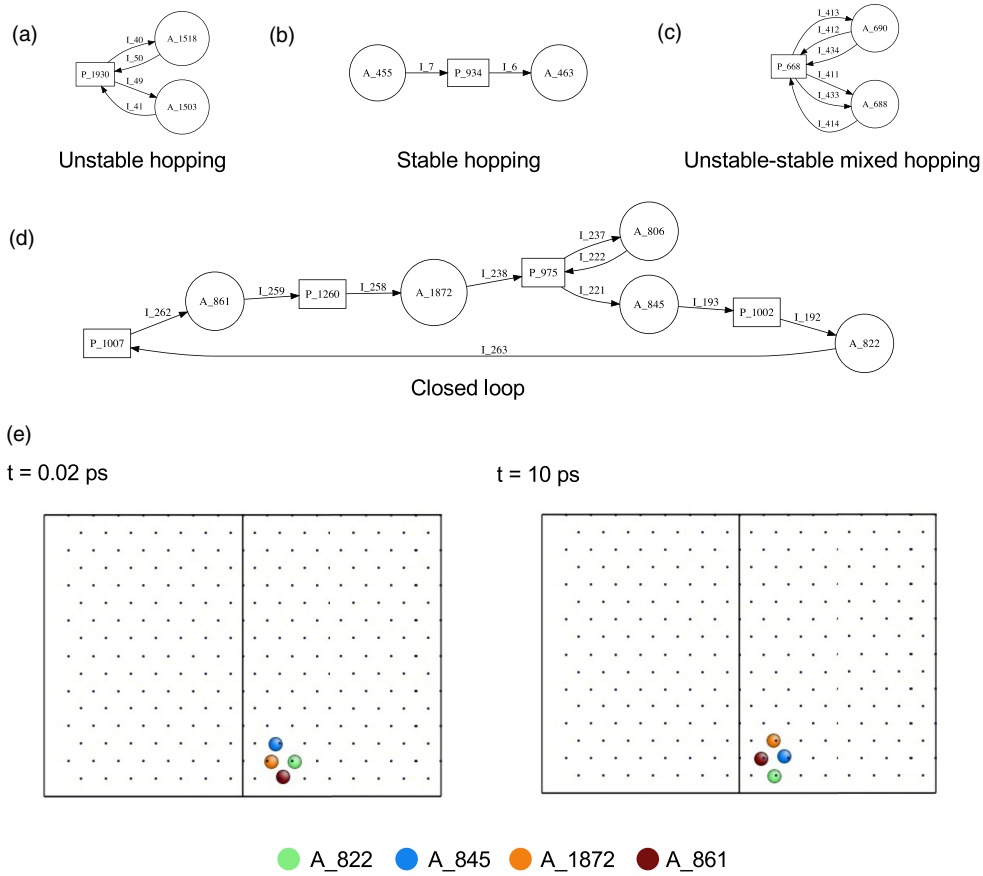


FIG. 5. Illustration of the hopping map schemes. In the hopping map, Position-ID, Atom-ID, and Image-ID are labeled as P_xxx, A_xxx, and I_xxx, respectively, where xxx are replaced with the index of their ID which is counted from zero. In this example, the system has 2048 atoms and 500 images. According to the final position of the atomic hopping, it can be classified as (a) unstable hopping which quickly returns to original position and (b) stable hopping which occupies new position permanently. When the two situations are both present, it is named (c) unstable-stable mixed hopping. (d) An example of the closed loop. Five atoms participated in the map, among which four atoms undergo stable (permanent) hopping, i.e., A_822, A_845, A_1872, A_861, while one atom undergoes unstable (temporary) hopping, i.e., A_806. (e) Snapshots of the movie that show the hopping mechanism of the closed loop viewed from the [110] direction, (left) initial state at $t = 0.02$ ps, (right) final state at $t = 10$ ps. Only atoms involved in the stable hoppings are highlighted with larger colored spheres, smaller black dots show the idealized positions of the perfect fcc crystal. The full version of the hopping map and movie can be found in the SM [35].

The two hopping situations could take place for the same group of atoms; thus, in that situation, it may be called a mixed hop [Fig. 5(c)]. Atoms pushed away by atoms that are permanently hopped will also permanently hop, causing a chain hop and forming a loop.

(4) According to the form of the loop, it can be divided into a closed loop and an open loop. Closed loop means that a cluster of atoms that have hopped during the observation period forms a closed path [Figs. 5(d) and 5(e)]. Open loop means that the atomic hopping has not yet formed a closed path during the observation period. An open loop can also be thought of as a closed loop in progress. As the observation time increases, the open loop may close finally, or multiple open loops may coalesce, leading to the formation of liquid nuclei, and eventually lead to melting. In this sense, the open loops can be regarded as the nucleation precursors of homogeneous melting.

(5) The transition state during the occurrence of atomic hopping can produce interstitial sites or vacancy defects; however, this transition state is inherently an unstable structure with a very short lifetime and disappears immediately upon formation.

In contrast to static defect models (e.g., vacancy-mediated or interstitial-mediated model [58]), the self-diffusion motion (loops or rings) mediated model is a dynamic defect model. When perfect crystals are strongly superheated, the dynamic defects, acting as precursors of melting before formation and growth of liquid nuclei, appear and disappear repeatedly and randomly in time and space. Notably, the dynamic defect model described above has been discovered by previous simulation studies [25,59,61], although there are some differences in the methods used to capture the information about atomic hopping. At present, a mature theory that connects the superheat limit and the atomic microscopic motion is still an open question. As demonstrated in the pioneering simulation studies, statistics on the form and number of dynamic defects can provide many valuable results. No doubt, more detailed, systematic research needs to be done next. In that research, we believe that the thermodynamic definition of the superheating limit proposed in this paper, a method of constructing the

thermodynamic surface, and thermodynamic quantities obtained by the thermodynamic surface approach (among which entropy may be the most important one as it plays a special role in linking the macroscopic property and microscopic states of substances), may serve as essential information for revealing the microscopic mechanism of homogeneous melting ultimately.

## IV. CONCLUSION AND PERSPECTIVES

In conclusion, we can present our answer to the question posed at the beginning of this paper. Considering the equilibrium thermodynamic changes, the metastable limit of homogeneous melting is the state at which one type of the superheated crystalline phase's thermodynamic potential reaches a critical value, which is equivalent to the value of the liquid phase referring to the state where heterogeneous freezing begins. Depending on whether homogeneous melting occurs under an isochoric or an isobaric condition, the thermodynamic potential is the internal energy or the enthalpy, respectively. Although some works have been conducted to explore the nucleation process of homogeneous melting and found that the assumption of the classical nucleation theory (CNT) is violated at the strong superheating regime [3], the microscopic mechanism of the initial incubation stage of the liquid nucleus in the vicinity of the superheat limit is still under debate [57–62,64]. Therefore, an unambiguous definition and determination of the superheating limit are crucial for investigating the fundamental mechanism of crystal melting. We believe that our findings in this work may serve as essential information for unraveling such a mechanism. In the past, examining this question was primarily of theoretical interest since superheating of a crystal is rarely achieved at the macroscopic scale. However, as demonstrated in the example of ultrafast logic devices based on phase-change materials (PCMs) [9], this situation is rapidly changing due to the advancement of assembly and fabrication technologies at the nanometer scale. This implies that the knowledge about the limit of superheating of crystals might be of practical use in many nanoscale engineering disciplines, for which the properties of superheated crystalline materials are predominant. Finally, because of its strength in interpreting and predicting the correlations between different melting simulation methods, we expect that the Gibbs thermodynamic surface approach adopted in this study will be useful for improving the efficiency in calculating the melting properties of substances from first principles, which will have broad applications in the geophysical, planetary, and material sciences.

## ACKNOWLEDGMENTS

This work was supported by the National Natural Science Foundation of China (Grants No. 41402033 and No. 41425009) and National Basic Research Program of China (Grant No. 2014CB845905). The numerical calculations were performed using the facilities at the High Performance Computing Center (HPCC) of Nanjing University and National Supercomputer Center in Guangzhou of China. K.Y. acknowledges the financial support from the China Scholarship Council (Grant No. 201406195030) for the visit to Sweden and thanks A. B. Belonoshko at the KTH Royal Institute of Technology for the stimulating discussions and comments on this work.

[1] J. G. Dash, Rev. Mod. Phys. **71**, 1737 (1999).
[2] Q. Mei and K. Lu, Prog. Mater. Sci. **52**, 1175 (2007).
[3] F. Wang, D. Zhou, and Y. Han, Adv. Funct. Mater. **26**, 8903 (2016).
[4] R. W. Cahn, Nature (London) **334**, 17 (1988).
[5] R. W. Cahn, Nature (London) **342**, 619 (1989).
[6] R. W. Cahn, Nature (London) **413**, 582 (2001).
[7] P. G. Debenedetti, *Metastable Liquids: Concepts and Principles* (Princeton University Press, Princeton, NJ, 1996).
[8] Y. Celik, L. A. Graham, Y.-F. Mok, M. Bar, P. L. Davies, and I. Braslavsky, Proc. Natl. Acad. Sci. U. S. A. **107**, 5423 (2010).
[9] D. Loke, J. M. Skelton, W.-J. Wang, T.-H. Lee, and T.-C. Chong, Proc. Natl. Acad. Sci. U. S. A. **111**, 13272 (2014).
[10] J. W. M. Frenken and J. F. van der Veen, Phys. Rev. Lett. **54**, 134 (1985).
[11] R. W. Cahn, Nature (London) **323**, 668 (1986).
[12] A. M. Alsayed, M. F. Islam, J. Zhang, P. J. Collings, and A. G. Yodh, Science **309**, 1207 (2005).
[13] B. Li, F. Wang, D. Zhou, Y. Peng, R. Ni, and Y. Han, Nature (London) **531**, 485 (2016).
[14] S. Williamson, G. Mourou, and J. C. M. Li, Phys. Rev. Lett. **52**, 2364 (1984).
[15] J. W. Herman and H. E. Elsayed-Ali, Phys. Rev. Lett. **69**, 1228 (1992).
[16] B. J. Siwick, J. R. Dwyer, R. E. Jordan, and R. J. D. Miller, Science **302**, 1382 (2003).
[17] J. Daeges, H. Gleiter, and J. H. Perepezko, Phys. Lett. A **119**, 79 (1986).
[18] F. Banhart, E. Hernández, and M. Terrones, Phys. Rev. Lett. **90**, 185502 (2003).
[19] F. A. Lindemann, Phys. Z. **11**, 609 (1910).
[20] M. Born, J. Chem. Phys. **7**, 591 (1939).
[21] J. J. Gilvarry, Phys. Rev. **102**, 308 (1956).
[22] H. J. Fecht and W. L. Johnson, Nature (London) **334**, 50 (1988).
[23] W. Kauzmann, Chem. Rev. **43**, 219 (1948).
[24] J. L. Tallon, Nature (London) **342**, 658 (1989).
[25] L. C. Gallington and A. Bongiorno, J. Chem. Phys. **132**, 174707 (2010).
[26] A. B. Belonoshko, N. V. Skorodumova, A. Rosengren, and B. Johansson, Phys. Rev. B **73**, 012201 (2006).
[27] D. Alfè, C. Cazorla, and M. J. Gillan, J. Chem. Phys. **135**, 024102 (2011).
[28] J. W. Gibbs, Trans. Conn. Acad. **2**, 382 (1873).
[29] J. E. Lennard-Jones, Proc. R. Soc. London A **106**, 463 (1924).
[30] O. L. Anderson, J. Geophys. Res. **84**, 3537 (1979).
[31] S.-T. Lin, M. Blanco, and W. A. Goddard III, J. Chem. Phys. **119**, 11792 (2003).
[32] M. A. van der Hoef, J. Chem. Phys. **113**, 8142 (2000).

[33] J. K. Johnson, J. A. Zollweg, and K. E. Gubbins, Mol. Phys. **78**, 591 (1993).
[34] M. P. Desjarlais, Phys. Rev. E **88**, 062145 (2013).
[35] See Supplemental Material at http://link.aps.org/supplemental/10.1103/PhysRevB.98.144113 for the choice of the reference state, method of entropy calibration, details and results of the two-phase simulations and supporting figures and movies.
[36] S. Plimpton, J. Comput. Phys. **117**, 1 (1995).
[37] J. C. Maxwell, *Theory of Heat*, 4th ed. (Longmans, Green, and Co., London, 1875).
[38] K. R. Jolls and D. C. Coy, Ind. Eng. Chem. Res. **47**, 4973 (2008).
[39] D. Frenkel and B. Smit, *Understanding Molecular Simulation: From Algorithms to Applications*, 2nd ed. (Academic, San Diego, 2002).
[40] *Free Energy Calculations*, edited by C. Chipot and A. Pohorille (Springer, Berlin, 2007).
[41] D. Alfè, M. J. Gillan, and G. D. Price, Nature (London) **401**, 462 (1999).
[42] J. R. Morris, C. Z. Wang, K. M. Ho, and C. T. Chan, Phys. Rev. B **49**, 3109 (1994).
[43] A. B. Belonoshko, Geochim. Cosmochim. Acta **58**, 4039 (1994).
[44] E. R. Hernández, A. Rodriguez-Prieto, A. Bergara, and D. Alfè, Phys. Rev. Lett. **104**, 185701 (2010).
[45] C. Cazorla, D. Alfè, and M. J. Gillan, Phys. Rev. B **85**, 064113 (2012).
[46] C. Cazorla, M. J. Gillan, S. Taioli, and D. Alfè, J. Chem. Phys. **126**, 194502 (2007).
[47] J. R. Morris and X. Song, J. Chem. Phys. **116**, 9352 (2002).
[48] E. A. Mastny and J. J. de Pablo, J. Chem. Phys. **127**, 104504 (2007).
[49] J. M. G. Sousa, A. L. Ferreira, and M. A. Barroso, J. Chem. Phys. **136**, 174502 (2012).
[50] U. R. Pedersen, J. Chem. Phys. **139**, 104102 (2013).
[51] J. Bouchet, F. Bottin, G. Jomard, and G. Zérah, Phys. Rev. B **80**, 094102 (2009).
[52] A. J. C. Ladd and L. V. Woodcock, Chem. Phys. Lett. **51**, 155 (1977).
[53] E. G. Noya, C. Vega, and E. de Miguel, J. Chem. Phys. **128**, 154507 (2008).
[54] W. Mickel, S. C. Kapfer, G. E. Schröder-Turk, and K. Mecke, J. Chem. Phys. **138**, 044501 (2013).
[55] K. Lu and Y. Li, Phys. Rev. Lett. **80**, 4474 (1998).
[56] Z. H. Jin, P. Gumbsch, K. Lu, and E. Ma, Phys. Rev. Lett. **87**, 055703 (2001).
[57] Z. Wang, F. Wang, Y. Peng, and Y. Han, Nat. Commun. **6**, 6942 (2015).
[58] M. Forsblom and G. Grimvall, Nat. Mater. **4**, 388 (2005).
[59] X.-M. Bai and M. Li, Phys. Rev. B **77**, 134109 (2008).
[60] Z. Wang, F. Wang, Y. Peng, Z. Zheng, and Y. Han, Science **338**, 87 (2012).
[61] H. Zhang, M. Khalkhali, Q. Liu, and J. F. Douglas, J. Chem. Phys. **138**, 12A538 (2013).
[62] A. Samanta, M. E. Tuckerman, T.-Q. Yu, and W. E, Science **346**, 729 (2014).
[63] E. R. Gansner and S. C. North, Software Pract. Exp. **30**, 1203 (2000).
[64] F. Wang, Z. Wang, Y. Peng, Z. Zheng, and Y. Han, Soft Matter **14**, 2447 (2018).